DOI: 10.1002/chem.200701668

Direct Thermal Decomposition of Metal Nitrates in Octadecylamine to Metal Oxide Nanocrystals

Ding-Sheng Wang,[a] Ting Xie,[a] Qing Peng,[a] Shao-Yan Zhang,[b] Jun Chen,[b] and Ya-Dong Li*[a]

Abstract: We have developed a method for the synthesis of metal oxide nanocrystals with controllable shape and size, which is based on the direct thermal decomposition of metal nitrates in octadecylamine. Mn_3O_4 nanoparticles and nanorods with different lengths were synthesized by using manganese nitrate as the decomposition material. Other metal oxide nanocrystals such as NiO, ZnO, CeO_2, CoO, and Co_3O_4 were also prepared by this method. These nanocrystals were then assembled into 3D colloidal spheres by a surfactant-assisted self-assembly process. Subsequently, calcination was carried out to remove the surfactants to obtain mesoporous metal oxides, which show large pores, good crystallization, thermally stable pore mesostructures, and potential applications in various fields, especially in catalysis and lithium-ion batteries.

Keywords: colloidal sphere · Li-ion battery · mesoporous materials · metal oxides · nanocrystals

Introduction

The development of strategies for the synthesis of nanometer-size crystallites has been among the key research topics in the field of nanoscience, not only for the significant scientific interest in understanding the kinetics and thermodynamics process of crystal growth, but also for the novel properties of these nanomaterials that differ drastically from their bulk counterparts and their potential applications in many chemical and biological fields.[1–6] Metal oxides, as an important class of materials, have been intensively pursued in recent years because of their unique size-dependent electrical, optical and magnetic properties, which are expected to find useful applications in lithium-ion batteries, catalysis, magnetic storages, sensors, etc.[7–12]

There have been many methods for the synthesis of metal oxide nanocrystals.[13–23] Among them, the most successful is the thermolysis of various organometallic precursors (such as metal acetylacetonates, metal cupferronates, metal alkoxides, and metal carbonyls) in complex organic solvent systems, which is largely inspired by the success of the synthesis of high-quality semiconductor nanocrystals in nonaqueous media.[24–26] For example, Alivisatos et al. reported that γ-Fe_2O_3 nanocrystals were synthesized from the thermal decomposition of an iron cupferron complex.[13] Two years later, the Hyeon group also reported the synthesis of γ-Fe_2O_3 nanocrystals by using an organometallic compound, $Fe(CO)_5$, as the precursor.[15] In the following years, the Sun group synthesized nearly monodisperse Fe_3O_4, $CoFe_2O_4$, and $MnFe_2O_4$ nanocrystals by using metal acetylacetonates as the precursors in the presence of 1,2-hexadecanediol, oleylamine, and oleic acid in phenol ether.[16,18] In 2004, Peng et al. synthesized monodisperse magnetite nanocrystals by decomposing the iron-oleate complexes in 1-octadecene.[17] However, to meet the demand in future applications of metal oxide nanocrystals, there still requires much effort in the exploration of size, shape controllable synthetic process and general precursors.

In this paper, we develop a general strategy to synthesize various metal oxide nanocrystals, namely, direct thermal decomposition of metal nitrates in octadecylamine. This simple process can be described concisely in Equation (1):

$$M(NO_3)_x \xrightarrow{\text{octadecylamine}} MO_{x/2}(\text{nanocrystals}) + xNO_2 + x/4\,O_2 \quad (1)$$

[a] D.-S. Wang, T. Xie, Dr. Q. Peng, Prof. Y.-D. Li
Department of Chemistry, Tsinghua University
Beijing, 100084 (P. R. China)
Fax: (+86) 10-6278-8765
E-mail: ydli@mail.tsinghua.edu.cn

[b] S.-Y. Zhang, Prof. J. Chen
Institute of New Energy Material Chemistry, Nankai University
Tianjin, 300071 (P. R. China)

Supporting information for this article is available on the WWW under http://www.chemeurj.org/ or from the author.

As the surface of as-formed $MO_{x/2}$ nanocrystals is protected by octadecylamine, the particles are stable and well dispersed in most hydrophobic solvents. Then, these as-obtained nanocrystals are used as building blocks to construct mesostructures. Various mesoporous metal oxides prepared with the bottom-up process show large pores, good crystallization and thermally stable pore structures. Furthermore, their performances in lithium-ion batteries have been exhibited to demonstrate the potential applications of these mesoporous metal oxides.

Results and Discussion

Mn_3O_4 nanocrystals: We employed the decomposition of manganese nitrate as a model system for studying the growth of oxide nanocrystals with our facile method. Mn_3O_4 nanocrystals with different shape and size can be obtained by directly decomposing manganese nitrate in octadecylamine under controlled conditions (see the Experimental Section). The transmission electron microscopy (TEM) and high-resolution TEM (HRTEM) images as shown in Figure 1 were taken to determine the morphology of products. Figure 1A displays the as-synthesized particle-shaped Mn_3O_4 nanocrystals. The lattice fringes visible in the HRTEM image (Figure 1B) are indicative of the high crystallinity of these particles and the interplanar distance of 0.250 nm can be indexed to plane (211) of tetragonal phase Mn_3O_4. Figure 1C,D shows the TEM images of Mn_3O_4 nanorods with different size and the HRTEM image (Figure 1E) demonstrates that the rods are well crystallized. Figure 1F reveals the crystal-lattice image of an individual Mn_3O_4 nanorod. The measured spacing of the lattice planes are 0.237 and 0.205 nm, and are consistent with the separations of (004) planes and (220) planes of tetragonal phase Mn_3O_4. The plane (004) is perpendicular to the axis of nanorod, indicating that the nanorod grows along the [001] direction. An X-ray powder diffraction (XRD) experiment was carried out to determine the structure and composition of the sample. As shown in Figure 2, all the peaks in the pattern can be readily indexed to a pure tetragonal phase of Mn_3O_4 (JCPDS 24–0734). No peaks of any other compositions (such as MnO or MnO_2) are detected, indicating that Mn_3O_4 is the only product of decomposition of manganese nitrate in octadecylamine.

Based on the above TEM results, we can see that the shape and size of as-obtained Mn_3O_4 nanocrystals can be influenced by concentration of manganese nitrate, decomposition temperature, and reaction time. If the monomer concentration is low, as soon as the Mn_3O_4 nuclei are formed, they will be capped by ligands of octadecylamine quickly. Then the classical Ostwarld ripening process will take place and lead to the formation of Mn_3O_4 particles.[27,28] When the concentration increases, the system will have a higher chemical potential, which is in favor of the growth of elongated nanocrystals. This process is in accord with the theory proposed by Peng's group.[29–31] Additionally, when we decompose manganese nitrate at higher temperature and shorter time, the nucleation process of nanocrystals will be accelerated, whereas the growth process will be limited, leading to the formation of Mn_3O_4 nanocrystals with smaller size.

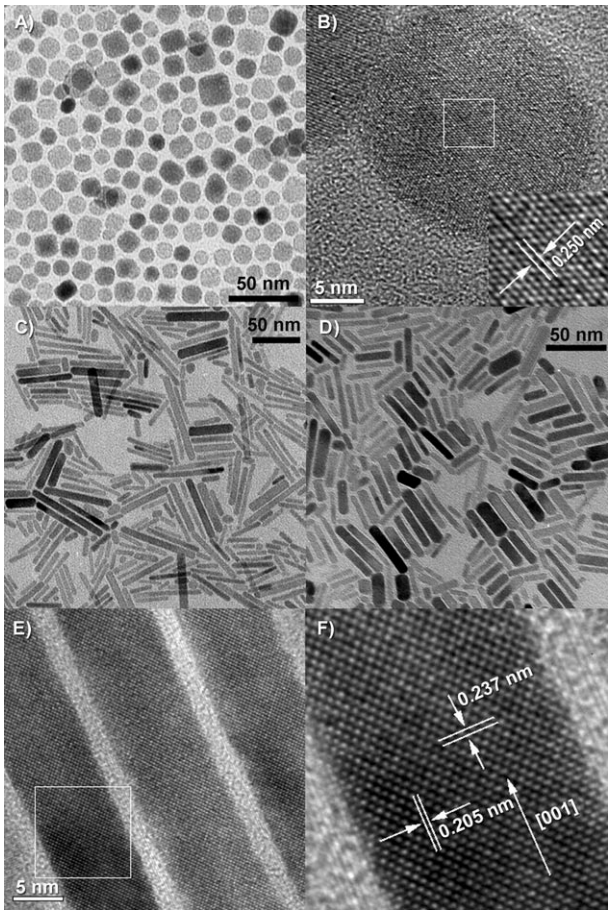

Figure 1. TEM and HRTEM images of Mn_3O_4 nanocrystals. A) Mn_3O_4 nanoparticles. B) HRTEM image of an individual Mn_3O_4 nanoparticle. C) Mn_3O_4 long nanorods. D) Mn_3O_4 short nanorods. E) HRTEM image of Mn_3O_4 nanorods. F) Crystal-lattice image of an individual Mn_3O_4 nanorod.

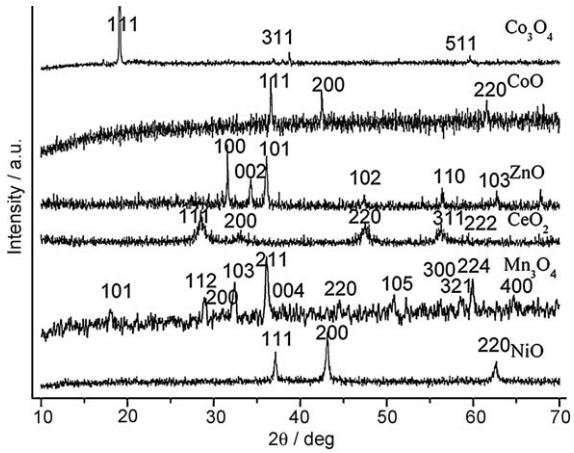

Figure 2. XRD patterns of as-prepared metal oxide nanocrystals.

Other metal oxide nanocrystals: The formation of other metal oxide nanocrystals was found to be very similar to that of Mn_3O_4 nanocrystals. XRD measurements (Figure 2) were used to prove the successful synthesis of these materials. TEM images shown in Figure 3 tell us that various metal oxides with unique morphologies can be prepared by this powerful method and the control of growth process of these nanocrystals can be achieved by modifying the reaction conditions. Figure 3A,B display the as-obtained NiO nanoflowers and ZnO triangular nanoplates with an average size of 20 and 100 nm, respectively, when we used nickel nitrate and zinc nitrate as the decomposition precursors separately. For CeO_2 nanocrystals, if we decompose cerium nitrate with a higher monomer concentration, at a higher temperature, and with a shorter time, then flower-shaped CeO_2 can be synthesized (Figure 3C), whereas if the reaction conditions are changed to that of lower monomer concentration, lower temperature, and longer time, we will obtain cube-shaped CeO_2 (Figure 3D). For the decomposition of cobalt nitrate, cobalt oxides with different compositions (CoO and Co_3O_4) and morphologies (polyhedron and cube) can be synthesized under different conditions. Figure 3E shows the TEM image of CoO nanopolyhedrons, and the inset displays the obvious polyhedral structure of the nanocrystals, while Figure 3F shows the TEM image of Co_3O_4 nanocubes, and the inset displays the self-assembly property of the nanocrystals.

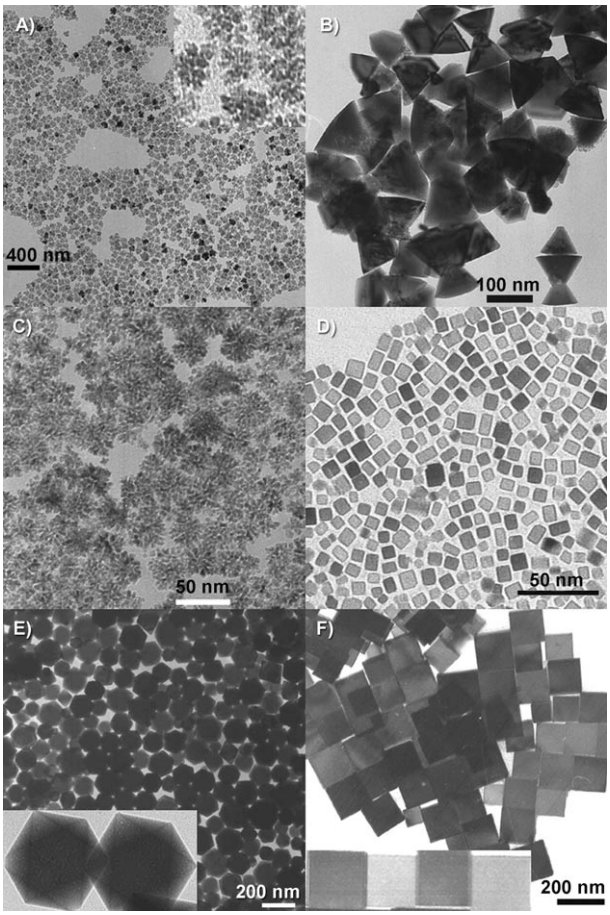

Figure 3. TEM images of metal oxide nanocrystals. A) NiO nanoflowers. B) ZnO triangular nanoplates. C) CeO_2 nanoflowers. D) CeO_2 nanocubes. E) CoO nanopolyhedrons. F) Co_3O_4 nanocubes.

From nanocrystals to colloidal spheres: After the synthesis of the various metal oxide nanocrystals, they were assembled into 3D colloidal spheres by means of a bottom-up self-assembly procedure (see Experimental Section) that has been developed by our group recently.[32] The XRD patterns (Supporting Information, Figure S1) demonstrate that the compositions of these metal oxides will not change during the assembly process and Figure 4 shows the TEM images of these colloidal spheres. Take NiO as an example, from Figure 4A we can see that this strategy can assemble NiO nanoflowers to colloidal spheres very effectively and no separate nanocrystals are found. It also can be clearly observed that the colloidal spheres are composed of nanocrystals from the TEM image of a single sphere (Figure 4A, inset). The as-obtained NiO spheres are polydisperse and the diameters range from 300 nm to 1.5 μm, which is also confirmed

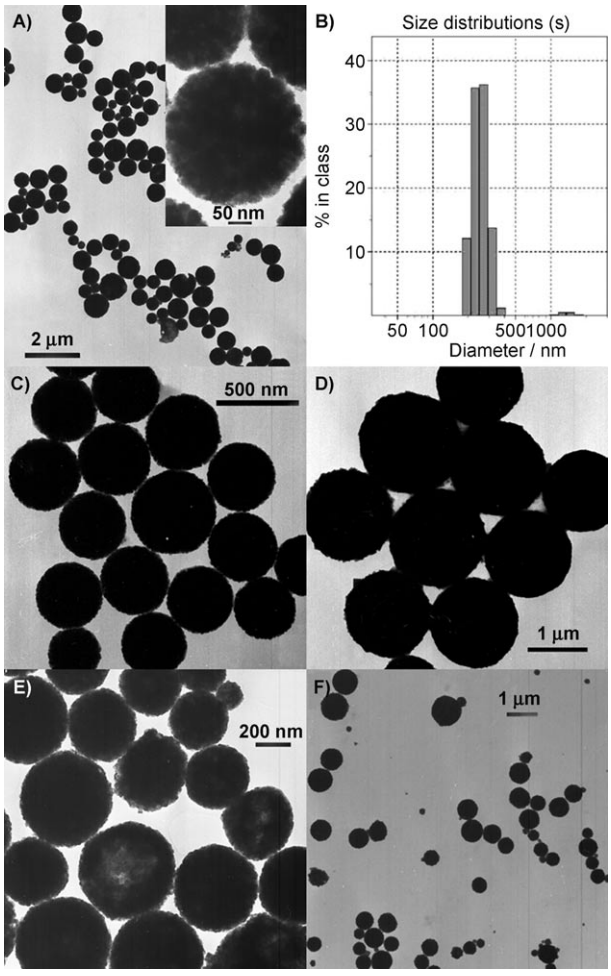

Figure 4. A) and C) TEM images of NiO colloidal spheres at different magnifications. B) DLS pattern of NiO spheres. D)–F) TEM images of CoO, Mn_3O_4, and CeO_2 colloidal spheres, respectively.

by the dynamic laser scattering (DLS) result (Figure 4B). However, we can separate them by centrifugation at different rotating speeds because there are obvious differences in the mass among various-sized spheres. Figure 4C shows the NiO spheres with smaller size (300–500 nm in diameter). Other metal oxide nanocrystals such as CoO nanopolyhedrons, Mn_3O_4 nanoparticles, and CeO_2 nanoflowers can also be assembled into their corresponding colloidal spheres. All of the products above are polydisperse and have diameters that range from 200 nm to 2 μm. We can obtain spheres with narrower size distribution by means of centrifuge separation, for example, CoO spheres with average diameter of 1 μm (Figure 4D), Mn_3O_4 spheres with average diameter of 300 nm (Figure 4E), and CeO_2 spheres with average diameter of 500 nm (Figure 4F).

Formation of mesoporous metal oxides: To obtain the mesoporous materials that have attracted intensive interest in recent years,[33–38] it is necessary to remove surfactants by calcining the as-prepared metal oxide colloidal spheres. If the spheres are calcined under Ar atmosphere, Mn_3O_4 will be reduced to MnO by carbon in the surfactants; NiO will also be partially reduced to Ni; whereas CoO can not be reduced. If this process is done in air, Mn_3O_4 and CoO will be oxidized to Mn_2O_3 and Co_3O_4 respectively, while NiO can keep the composition. These results are demonstrated by XRD measurements (Supporting Information, Figure S2). During calcination, both under Ar atmosphere and in air, the structures do not collapse. Figure 5 shows the scanning electron microscope (SEM) images of mesoporous NiO, MnO, and CoO materials. From their high-resolution SEM images, we can see clearly that the microspheres are made up of cumulate nanocrystal building blocks, resulting in the formation of large-pore mesoporous architectures. The N_2 adsorption–desorption data (Figure 6) from Brunauer–Emmett–Teller (BET) measurements and the corresponding Barrett–Joyner–Halenda (BJH) pore-size distribution data (Figure 6, insets) for NiO, MnO, Mn_2O_3, CoO, and Co_3O_4 materials show that mesopores exist in these materials. Their average pore diameters are 20, 10, 30, 30, and 20 nm indicated by pore size distribution curves.

To investigate the change of surface area for these metal oxides from nanocrystals to mesoporous structures, we first calcine the nanocrystals with the same conditions as corresponding mesoporous metal oxides, and then compare their BET surface area. The results are collected in Table 1, from which we can see that there is clear increase in surface area after the creation of mesoporous structures from nanocrystals. This is attributable to the removal of surfactants. Before calcination, the surfactants in the colloidal spheres occupied large space. This bottom-up procedure shows us a new idea and a novel synthetic strategy for mesoporous materials. A notable advantage of this method is that most nanocrystals can be used as building blocks and the assembly process is independent of their respective chemical compositions, which means that if we can get the nanocrystals of any material, then we can obtain their corresponding mesoporous products. We can even synthesis hybrid mesoporous materials by mixing two or more kinds of crystals in the assembly process and tune the pore size by controlling the size of nanocrystals (ongoing work in our group). Another advantage is the good crystallization and thermal stability of these mesoporous materials that shows promise for their potential applications in catalysis and lithium-ion batteries.

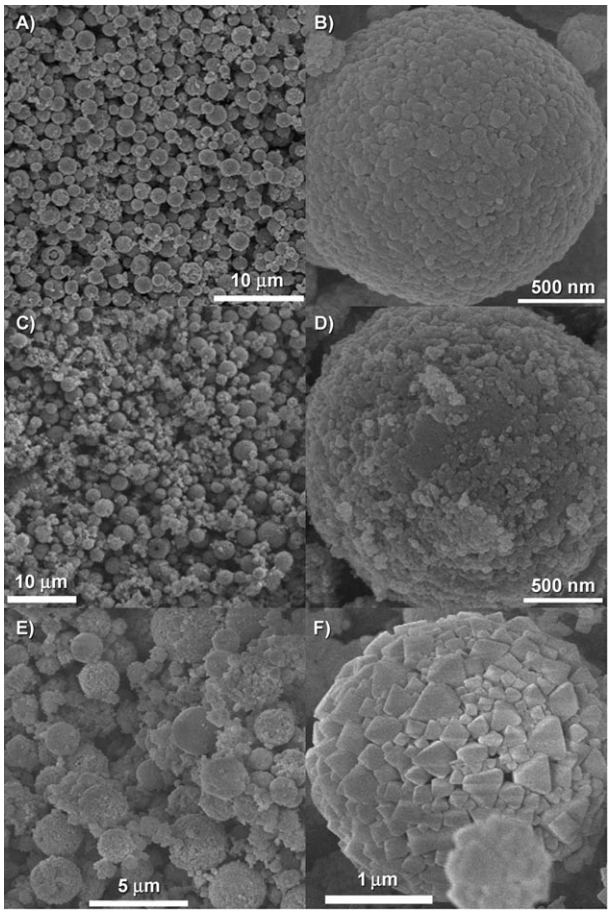

Figure 5. SEM images of the calcined products. A) and B) NiO. C) and D) MnO. E) and F) CoO.

Application in lithium-ion batteries: We selected their application in lithium-ion batteries to display the potential properties of these as-obtained mesoporous materials. As we all know, the MO (M = Ni, Co, Mn, etc.) type oxides demonstrate a large capacity, long cycle life, and high recharging rate as anode materials for Li-ion batteries.[39,40] Many efforts have been reported to develop their electrochemical performance.[41–45] The utilization of mesoporous metal oxides as electrodes might be a great help because of not only the larger surface area, but also the ease for the lithium ions to diffuse in the mesostructures. Figure 7 (bottom right inset) shows the cyclic voltammograms (CV) of the mesoporous NiO electrode in the first cycle. In the cathodic polarization process, a reduction peak ranging from 0.3–0.8 V attributes to the initial reduction of NiO to Ni and the formation of a partially reversible solid electrolyte interface (SEI)

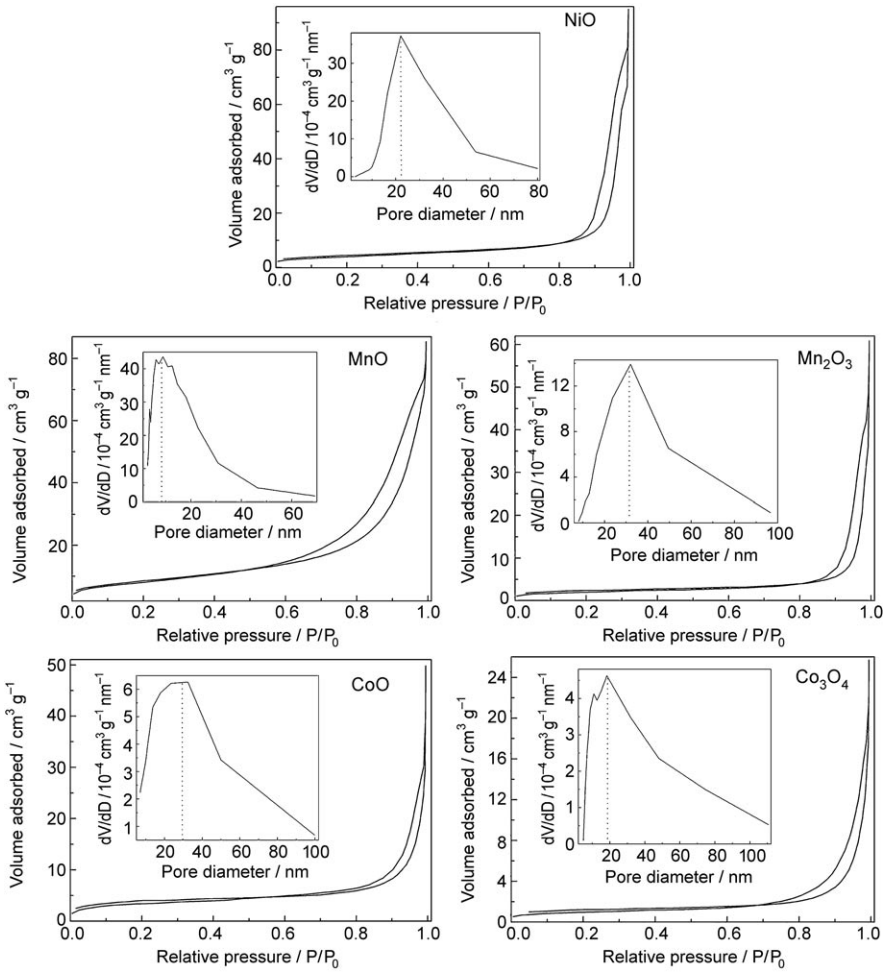

Figure 6. N_2 adsorption–desorption isotherm and corresponding pore size distribution curve (inset) for mesoporous metal oxides.

Table 1. The comparison of BET surface area between metal oxide nanoparticles and corresponding mesoporous structures.

Product (nanoparticles)	BET surface area [$m^2 g^{-1}$]	Product (mesoporous)	BET surface area [$m^2 g^{-1}$]
NiO[a]	12.1	NiO[b]	16.1
CoO[c]	3.3	CoO[d]	14.4
Mn_3O_4[c]	25.3	MnO[d]	30.6

[a] Calcining NiO nanoparticles in air at 350°C for 1 h followed by 500°C for 1 h . [b] Calcining NiO colloidal spheres in air at 350°C for 1 h followed by 500°C for 1 h. [c] Calcining CoO and Mn_3O_4 nanoparticles under Ar at 350°C for 1 h followed by 500°C for 1 h. [d] Calcining CoO and Mn_3O_4 colloidal spheres under Ar at 350°C for 1 h followed by 500°C for 1 h.

layer.[43] Meanwhile, in the anodic polarization process, one broad peak recorded at about 2.5 V corresponds to the oxidation of Ni to Ni^{2+}. Constant current charge/discharge measurements give us the voltage-specific capacity curve (Figure 7) of the NiO/Li cell, from which it can be seen that in the first discharge, the potential drops rapidly to reach a well-pronounced plateau at about 0.62 V, followed by a gradual decrease to 0.01 V. After the first five cycles, the NiO/Li cell reaches a steady state and the capacity nearly remains constant over 30 cycles (Figure 7, top left inset). The details how the mesostructures influence the performance of metal oxide electrodes and how to adjust the experimental conditions to develop their electrochemical properties to meet with the industrial demands require further investigation. Corresponding studies are underway in our group. For example, hybrid mesoporous materials combining NiO, CoO, and MnO are expected to be prospective electrodes.

Conclusion

In summary, we have developed a simple and general method to synthesize metal oxide nanocrystals, namely, direct thermal decomposition of nitrate salts in octadecylamine, which is a rapid, economical, and easily scaled up method for nanocrystals. Then, these as-obtained metal oxide nanocrystals are used as building blocks to construct mesoarchitectures. This bottom-up self-assembly procedure opens a novel path for the fabrication

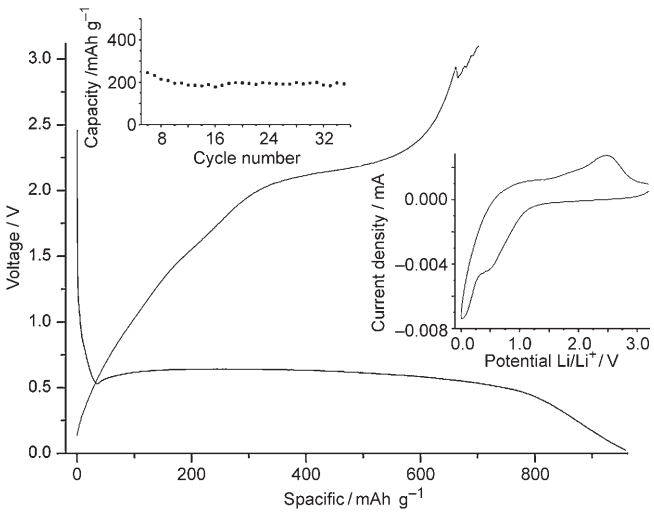

Figure 7. Charge-discharge curve of the NiO/Li cell. The top left and bottom right insets show the cycle life of the cell and the cyclic voltammograms of the electrode made by mesoporous NiO.

of well-crystallized mesoporous materials. Various mesoporous metal oxides have been successfully synthesized and the application in lithium-ion batteries has also been examined briefly. Ongoing work shows the possibility of preparing mesoporous metals, sulfides, fluorides, phosphides, and so forth, and tuning the pore size from micro to meso even macro, as well as fabricating hybrid mesoporous materials. The tremendous potentiality in catalysis application is also being studied in our group. We believe that it would be a significant advance for material science and probably a bringing of new developments in this area.

Experimental Section

Materials: All the reagents used in this work, including manganese nitrate, nickel nitrate, cerium nitrate, zinc nitrate, cobalt nitrate, octadecylamine, ethanol, and cyclohexane were of A.R. grade from the Beijing Chemical Factory, China.

Synthesis

Mn_3O_4 nanoparticles: 0.1 mL of $Mn(NO_3)_2$ solution (50 wt%) was added to 10 mL octadecylamine at 200°C. After 10 min of magnetic stirring, the system was allowed to cool to 80°C (the melting point of octadecylamine) and the final products collected at the bottom of the beaker. The Mn_3O_4 nanoparticles were washed with ethanol several times, and then dispersed into a non-polar solvent, such as cyclohexane.

Mn_3O_4 long nanorods: 1 mL of $Mn(NO_3)_2$ solution (50 wt.%) was added to 10 mL octadecylamine at 200°C. After 10 min of magnetic stirring, Mn_3O_4 long nanorods were collected and washed.

Mn_3O_4 short nanorods: 3 mL of $Mn(NO_3)_2$ solution (50 wt.%) was added into 10 mL octadecylamine at 220°C. After 1 min of magnetic stirring, Mn_3O_4 short nanorods were collected and washed.

NiO nanoflowers: 1 g of $Ni(NO_3)_2{\cdot}6H_2O$ was added to 10 mL octadecylamine at 180°C. After 10 min of magnetic stirring, NiO nanoflowers were collected and washed.

ZnO triangular nanoplates: 0.2 g $Zn(NO_3)_2{\cdot}6H_2O$ was added into 10 mL octadecylamine at 200°C. After 10 min of magnetic stirring, ZnO triangular nanoplates were collected and washed.

CeO_2 nanoflowers: 1 g of $Ce(NO_3)_3{\cdot}6H_2O$ was added into 10 mL octadecylamine at 250°C. After 8 min of magnetic stirring, CeO_2 nanoflowers were collected and washed.

CeO_2 nanocubes: 0.2 g of $Ce(NO_3)_3{\cdot}6H_2O$ was added into 10 mL octadecylamine at 120°C. After 2 min of magnetic stirring, the system was kept at 200°C for 24 h. Then, CeO_2 nanocubes were collected and washed.

CoO nanopolyhedrons: 0.5 g $Co(NO_3)_2{\cdot}6H_2O$ was added into 10 mL octadecylamine at 250°C. After 20 min of magnetic stirring, CoO polyhedrons were collected and washed.

Co_3O_4 nanocubes: 1 g $Co(NO_3)_2{\cdot}6H_2O$ was added into 10 mL octadecylamine at 120°C. After 5 min of magnetic stirring, the system was kept at 200°C for 24 h. Then, Co_3O_4 nanocubes were collected and washed.

Colloidal spheres: The following is a typical synthetic procedure for colloidal spheres: 0.3 g of sodium dodecylsulfonate (SDS) was dissolved into 100 mL of deionized water, and then 10 mL of metal oxide nanocrystal solution ($\approx$10 mg/mL, the solvent is cyclohexane) was added. The solution was magnetically stirred at room temperature for 1 h, and then heated to 80°C and stirred for a further 1 h to evaporate the cyclohexane. The metal oxide colloidal spheres were obtained by centrifuging and washing with water.

Mesoporous metal oxides: Mesoporous materials would be obtained by calcining the as-synthesized colloidal spheres. For mesoporous NiO, Mn_2O_3, and Co_3O_4, we calcined NiO, Mn_3O_4, and CoO colloidal spheres in air at 350°C for 1 h followed by 500°C for 1 h. For mesoporous MnO and CoO, we calcined Mn_3O_4 and CoO colloidal spheres under Ar at 350°C for 1 h followed by 500°C for 1 h.

Characterization: A Bruker D8-advance X-ray powder diffractometer with $Cu_{K\alpha}$ radiation ($\lambda = 1.5418$ Å) was used for the characterization of phase purity and crystallinity of the products. A Hitachi H-800 transmission electron microscope (TEM) was used to measure the size and morphology of all the samples. Scanning electron microscopy (SEM) images were taken by means of a JSM-6310F scanning electron microscope. Dynamic laser scattering (DLS) was used to measure the size distribution of colloidal spheres. The BET surface area of samples was measured by using N_2 adsorption with the single-point method.

Electrochemical measurement: Electrochemical measurements were carried out by using two-electrode cells with lithium metal as the counter electrode. The working electrodes were fabricated by compressing the mixture of 85 wt% active materials, 10 wt% acetylene black, and 5 wt% ploytetrafluoroethylene. The electrolyte solution was $LiPF_6$ (1 M) dissolved in a mixture of ethylene carbonate (EC), propylene carbonate (PC), and diethyl carbonate (DEC) with the volume ratio of EC/PC/DEC = 3:1:1. Electrochemical performance was investigated by using a Solartron SI 1260 Potentionstat Analyzer with 1287 Interface and a modified Arbin charge-discharge unit at controlled temperatures.

Acknowledgements

This work was supported by NSFC (90606006), the Foundation for the Author of National Excellent Doctoral Dissertation of China and the State Key Project of Fundamental Research for Nanoscience and Nanotechnology (2006CBON0300), the Key grant Project of the Chinese Ministry of Education (NO. 306020).

[1] A. P. Alivisatos, *Science* **1996**, *271*, 933.
[2] C. B. Murray, C. R. Kagan, M. G. Bawendi, *Annu. Rev. Mater. Sci.* **2000**, *30*, 545.
[3] C. N. R. Rao, G. U. Kulkarni, P. J. Thomas, P. P. Edwards, *Chem. Eur. J.* **2002**, *8*, 29.
[4] J. Park, K. J. An, Y. S. Hwang, J. G. Park, H. J. Noh, J. Y. Kim, J. H. Park, N. M. Hwang, T. Hyeon, *Nat. Mater.* **2004**, *3*, 891.
[5] C. Burda, X. Chen, R. Narayanan, M. A. El-Sayed, *Chem. Rev.* **2005**, *105*, 1025.
[6] Y. P. Du, Y. W. Zhang, Z. G. Yan, L. D. Sun, S. Gao, C. H. Yan, *Chem. Asian J.* **2007**, *2*, 965.
[7] J. M. Tarascon, M. Armand, *Nature* **2001**, *414*, 359.
[8] V. Kesavan, D. Dhar, Y. Koltypin, N. Perkas, O. Palchik, A. Gedanken, S. Chandersekaran, *Pure Appl. Chem.* **2001**, *73*, 85.
[9] N. Pinna, G. Neri, M. Antonietti, M. Niederberger, *Angew. Chem.* **2004**, *116*, 4445; *Angew. Chem. Int. Ed.* **2004**, *43*, 4345.
[10] A. A. Khaleel, *Chem. Eur. J.* **2004**, *10*, 925.
[11] J. P. Ge, Y. X. Hu, M. Biasini, W. P. Beyermann, Y. D. Yin, *Angew. Chem.* **2007**, *119*, 4420; *Angew. Chem. Int. Ed.* **2007**, *46*, 4342.
[12] R. Murugan, V. Thangadurai, W. Weppner, *Angew. Chem. Int. Ed.* **2007**, *46*, 7778.
[13] J. Rockenberger, E. C. Scher, A. P. Alivisatos, *J. Am. Chem. Soc.* **1999**, *121*, 11595.
[14] J. J. Schneider, N. Czap, J. Hagen, J. Engstler, J. Ensling, P. Gütlich, U. Reinoehl, H. Bertagnolli, F. Luis, L. Jos de Jongh, M. Wark, G. Grubert, G. L. Hornyak, R. Zanoni, *Chem. Eur. J.* **2000**, *6*, 4305.
[15] T. Hyeon, S. S. Lee, J. Park, Y. Chang, H. B. Na, *J. Am. Chem. Soc.* **2001**, *123*, 12798.
[16] S. Sun, H. Zeng, *J. Am. Chem. Soc.* **2002**, *124*, 8204.
[17] N. R. Jana, Y. F. Chen, X. G. Peng, *Chem. Mater.* **2004**, *16*, 3931.
[18] S. Sun, H. Zeng, D. B. Robinson, S. Raoux, P. M. Rice, S. X. Wang, G. Li, *J. Am. Chem. Soc.* **2004**, *126*, 273.
[19] X. Wang, J. Zhuang, Q. Peng, Y. D. Li, *Nature* **2005**, *437*, 121.
[20] J. Du, Y. Q. Gao, L. L. Chai, G. F. Zou, Y. Li, Y. T. Qian, *Nanotechnology* **2006**, *17*, 4923.

[21] L. P. Zhou, J. Xu, X. Q. Li, F. Wang, *Mater. Chem. Phys.* **2006**, *97*, 137.
[22] A. Narayanaswamy, H. F. Xu, N. Pradhan, X. G. Peng, *Angew. Chem.* **2006**, *118*, 5487; *Angew. Chem. Int. Ed.* **2006**, *45*, 5361.
[23] M. Niederberger, G. Garnweitner, *Chem. Eur. J.* **2006**, *12*, 7282.
[24] C. B. Murray, D. J. Norris, M. G. Bawendi, *J. Am. Chem. Soc.* **1993**, *115*, 8706.
[25] X. G. Peng, J. Wickham, A. P. Alivisatos, *J. Am. Chem. Soc.* **1998**, *120*, 5343.
[26] X. G. Peng, L. Manna, W. D. Yang, J. Wickham, E. Scher, A. Kadavanich, A. P. Alivisatos, *Nature* **2000**, *404*, 59.
[27] C. B. Murray, C. R. Kagan, M. G. Bawendi, *Annu. Rev. Mater. Sci.* **2000**, *30*, 545.
[28] A. L. Rogach, D. V. Talapin, E. V. Shevchenko, A. Kornowski, M. Haase, H. Weller, *Adv. Funct. Mater.* **2002**, *12*, 653.
[29] Z. A. Peng, X. G. Peng, *J. Am. Chem. Soc.* **2002**, *124*, 3343.
[30] X. G. Peng, *Chem. Eur. J.* **2002**, *8*, 335.
[31] X. G. Peng, *Adv. Mater.* **2003**, *15*, 459.
[32] F. Bai, D. S. Wang, Z. Y. Huo, W. Chen, L. P. Liu, X. Liang, C. Chen, X. Wang, Q. Peng, Y. D. Li, *Angew. Chem. Int. Ed.* **2007**, *46*, 6650.
[33] D. Y. Zhao, J. L. Feng, Q. S. Huo, N. Melosh, G. H. Fredrickson, B. F. Chmelka, G. D. Stucky, *Science* **1998**, *279*, 548.
[34] P. D. Yang, D. Y. Zhao, D. I. Margolese, B. F. Chmelka, G. D. Stucky, *Nature* **1998**, *396*, 152.
[35] P. D. Yang, T. Deng, D. Y. Zhao, P. Y. Feng, D. Pine, B. F. Chmelka, G. M. Whitesides, G. D. Stucky, *Science* **1998**, *282*, 2244.
[36] A. S. Deshpande, N. Pinna, B. Smarsly, M. Antonietti, M. Niederberger, *Small* **2005**, *1*, 313.
[37] Y. F. Lu, *Angew. Chem.* **2006**, *118*, 7826; *Angew. Chem. Int. Ed.* **2006**, *45*, 7664.
[38] X. Y. Lai, X. T. Li, W. C. Geng, J. C. Tu, J. X. Li, S. L. Qiu, *Angew. Chem.* **2007**, *119*, 752; *Angew. Chem. Int. Ed.* **2007**, *46*, 738.
[39] P. Poizot, S. Laruelle, S. Grugeon, L. Dupont, J. M. Tarascon, *Nature* **2000**, *407*, 496.
[40] M. S. Whittingham, *Chem. Rev.* **2004**, *104*, 4271.
[41] Y. G. Li, B. Tan, Y. Y. Wu, *J. Am. Chem. Soc.* **2006**, *128*, 14258.
[42] J. Y. Luo, J. J. Zhang, Y. Y. Xia, *Chem. Mater.* **2006**, *18*, 5618.
[43] S. Laruelle, S. Grugeon, P. Poizot, M. Dollé, L. Dupont, J. M. Tarascon, *J. Electrochem. Soc.* **2002**, *149*, A627.
[44] L. Yuan, Z. P. Guo, K. Konstantinov, P. Munroe, H. K. Liu, *Electrochem. Solid-State Lett.* **2006**, *9*, A524.
[45] X. H. Huang, J. P. Tu, C. Q. Zhang, X. T. Chen, Y. F. Yuan, H. M. Wu, *Electrochim. Acta* **2007**, *52*, 4177.

Received: October 23, 2007
Published online: January 11, 2008

